Filtering of FTLE for Visualizing Spatial Separation in Unsteady 3D Flow

Armin Pobitzer, Ronald Peikert, Raphael Fuchs, Holger Theisel, and Helwig Hauser

Abstract In many cases, feature detection for flow visualization is structured in two phases: first candidate identification, and then filtering. With this paper, we propose to use the directional information contained in the *finite-time Lyapunov exponents* (FTLE) computation, in order to filter the FTLE field. Thereby we can focus on those separation structures that delineate flow compartments which develop into different spatial locations, as compared to those that separate parallel flows of different speed. We provide a discussion of the underlying theory and our related considerations. We derive a new filtering scheme and demonstrate its effect in the context of several selected fluid flow cases, especially in comparison with unfiltered FTLE visualization. Since previous work has provided insight with respect to the studied flow patterns, we are able to provide a discussion of the resulting visible separation structures.

1 Introduction

The concept of flow plays a central role in many fields. Classical application fields are the automotive and aviation industries. The visualization of data gained from the simulation or measurement of flow processes is relevant for the domain users, as visualization has the potential to ease the understanding of complex flow phenomena.

For a good overall understanding of the flow, the identification of areas with coherent flow behavior has proved to be useful. For steady flow, methods based on *vector field topology*, as introduced to the visualization community by Helmann

Armin Pobitzer and Helwig Hauser
University of Bergen, Norway, e-mail: {armin.pobitzer,helwig.hauser}@uib.no

Ronald Peikert and Raphael Fuchs
ETH Zurich, Switzerland e-mail: {peikert,raphael}@inf.ethz.ch

Holger Theisel
University of Magdeburg, Germany e-mail: theisel@isg.cs.uni-magdeburg.de

and Hesselink [17], provide an expressive segmentation of the flow. In the case of unsteady flow, a comparable theory is not readily available, even though a number of promising approaches and methods have been worked out in the past years. We refer to a related state of the art report [25] for an overview of topology-based methods for the visualization of unsteady flow.

One of the promising directions leading to a semantic segmentation of unsteady flow, are so-called *Lagrangian* methods. These methods focus on the motion of massless particles in the flow. The most prominent methods are related to *finite-time Lyapunov exponents* (FTLE). Haller [13, 14] shows the relation of FTLE to *Lagrangian coherent structures* and its application to flow data.

Roughly speaking, the (maximum) FTLE gives the maximum separation rate for nearby particles over a certain time-period. When interpreting separation structures extracted from the FTLE field, such as ridges, this concept of separation, has to be kept in mind: Apart from the separation due to differences in flow directions, FTLE will also detect separation due to differences in flow magnitude. We illustrate this with a simple thought experiment:

We consider two particles that travel on straight parallel lines with constant velocity, but the one velocity being larger the other. At a certain time, these particles have a certain distance from each other. The distance between the particles increases monotonically (due to the different particle velocities), but their paths remain nonetheless parallel, leading the particles into the same area (but at different times). Fig. 1 illustrates this situation.

This causes, for example, that a shear layer is a region with high FTLE values. More generally, regions of particles with parallel paths but different speeds will show this behavior. A separation concept that is not sensitive to such differences in speed would therefore define particles as "staying close" if their paths stay nearby. This concept of vicinity is called *Poincaré* or *orbital stability*. Formally, a path line is Poincaré stable if for any given $\varepsilon > 0$, there is a $\delta > 0$ such that a particle with starting distance δ to the path line stays in the ε-tube around it [19]. Although well known in theory, the definition of Poincaré stability does not provide an intuitive quantification of distance (since it would require to compare every single point on one path to all points on the other path).

From the above mentioned thought experiment we infer that separation resulting from differences in the velocity magnitude, occurs along the lines, i.e., in direction of the flow vector, while separations due to differences in flow direction will occur at an angle to the flow direction. The analysis of the deformation gradient tensor builds on the assumption of a linear mapping between the difference of the particle positions before and after advection by the flow and assumes hence that the distance between particles is locally describable by straight lines [22]. Hence, our considerations are valid for arbitrary path lines, as long as the general assumptions for the FTLE analysis are fulfilled.

The direction of the main separation can be found by analyzing the *gradient of the flow map* (in a more general setting referred to as the *deformation gradient tensor* [22]). For this purpose we usef *singular value decomposition* (SVD). We show in section 3 that our approach is directly derived from the geometric approach

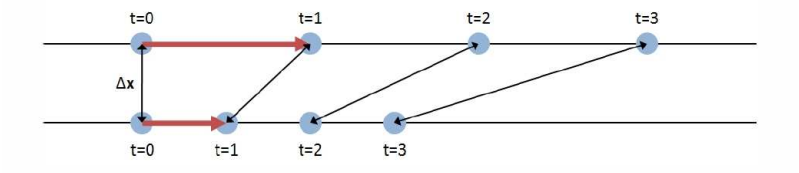

Fig. 1 Two particles traveling along straight parallel lines at different speeds: we see that the particles separate in the direction of the movement, but their paths are at a fixed distance, and will hence traverse the same regions.

to FTLE as provided by Haller [13]. The examination of the angle between this main separation direction and the direction of the path line gives us a measure for the spatial separation that is represented by the respective FTLE values. Filtering the FTLE field with this measure then yields the separation structures representing a separation inspired by Poincaré stability. One needs to be aware of this different stability – and hence, separation – concept, and assess its meaningfulness in the case under investigation.

Accordingly, the main contribution of this paper is a new filter, to be used as a filtering step after the computation of FTLE values in unsteady flow fields, that allows to focus on those regions within the flow that lead to spatial separation.

The remainder of this paper is structured as follows: First we discuss related work. Then we introduce our proposed filtering approach, deriving it from the known theory. In the subsequent section we present results from analyzing several flow cases, applying our filtering to four simple analytical examples, the well-known "double gyre" example by Shadden et al. [29], and a CFD data set demonstrating what results we can achieve. We then discuss computational aspects of the estimation of the deformation gradient tensor and the extraction of the main separation direction. Finally we discuss results and point out future work.

2 Related Work

The visualization of flow is an active research field. Topological methods were first introduced to the scientific visualization community by Helman and Hesselink [17, 18] for both 2D and 3D steady flow fields, under the notion of *vector field topology* (VFT). Globus et al. [10] showed the practical relevance of VFT for computational fluid dynamics data. For a detailed survey of VFT for two and three dimensions we refer to Asimov's tutorial [1].

From the theoretical point of view, the applicability of VFT for unsteady flow has been questioned, among others, by Perry and Chong [24]. They conclude that classical VFT is only applicable to nearly steady fields. Later Shadden [29] and Wiebel et al. [33] showed this by specific examples. Very recently, Fuchs et al. [6]

proposed an extended critical point concept which allows them to apply vector field topology in the case of unsteady flow.

Theisel et al. [31] introduce flow topology based on path lines. Path lines are the paths of massless particles that are advected by the flow. Therefore, they are inherently well suited to gain an understanding of unsteady flow.

The seminal paper of Haller [13] introduces FTLE to the analysis of flow fields. The concept of *Lagrangian coherent structures* (LCS) is discussed and its connection to FTLE is revealed. LCS are – to a certain degree – the unsteady analogon of separatrices in VFT. In a follow-up paper [14], Haller showed that LCS correspond to ridges of the FTLE field. Sadlo et al. [27] and Shi et al. [30] compare LCS to VFT and conclude that the information conveyed by FTLE is only partial as compared to VFT, missing out, for example, on vortices.

The standard algorithm for the computation of the FTLE field involves the seeding of a large number of particles in the flow and the calculation of their path lines (flow map). This is computationally challenging since it requires a high precision integration for every particle. Sadlo and Peikert [26] use adaptive mesh refinement in their ridge extraction to avoid unnecessary evaluations of the flow map. As shown by Shadden [29], LCS are "nearly" material lines. This can be exploited to speed up the algorithm. Sadlo et al. [28] present a method to extract LCS using grid advection, exploiting the temporal coherency of LCS. Lipinski and Mohseni [21] present a ridge tracking algorithm for FTLE fields that uses both temporal and spatial coherency of LCS, and give an error estimator for the difference between the advected ridge the and actual LCS. Both approaches give great speed-up compared to the standard algorithm.

As the computation of ridges usually involves the computation of higher-order derivatives, the computation will be sensitive to noise. Furthermore, some types of solvers used to simulate the flow, e.g., *spectral element methods* [32], may introduce discontinuities in higher-order derivatives.

Garth et al. [7] avoid the computation of ridges using a volume rendering approach. The authors show also that 3D FTLE might be approximated by 2D FTLE in selected cross-sections. Furthermore, the authors present an efficient approximation to FTLE fields.

Kasten et al. [20] introduce the notion of *localized FTLE* (L-FTLE). The main idea of this approach is to exchange the deformation gradient tensor with a matrix that accumulates the separation behavior along a path line. Haller and Sapsis [15] show that also the smallest FTLE is related to LCS, and can be used to compute the attracting LCS from forward standard FTLE (and vice versa). This makes computing both forward and backward FTLE obsolete and, hence, saves costly computations.

To the best of our knowledge, no attempts have been made yet to use the directional information inherent to the definition of FTLE in visualization. Obermaier et al. [23] use iteratively deformed ellipsoids to visualize volume deformation along trajectories. The deformation in every iteration step is analyzed using *Singular Value Decomposition* (SVD), which also our approach makes use of. It is worthwhile noticing that their approach imposes divergence-freeness.

3 The filtering scheme

In the following, we show how the main separation direction can be computed from the directional information that is inherent to the definition of FTLE and how it can be easily derived from it.

Definition of FTLE and its geometric interpretation: The concept of *finite-time Lyaponov exponents* (FTLE) is an adaptation of the concept of the classical Lyapunov exponents to the situation of a vector field which is defined over finite time only. Those fields are of practical relevance since both simulations and measurements of unsteady flow will typically yield this type of fields. Roughly speaking, the FTLE is the maximum deformation of a small neighborhood advected by the flow over a certain time-interval. This maximum deformation can be computed from the maximum eigenvalue of the (right) Cauchy-Green tensor [22, 13].

In the original paper [13], Haller gives an alternative, geometric reasoning to motivate the interpretation of the FTLE field, which yields the same formula as the standard formulation. We will use this reasoning as a starting point for our own considerations: Let $\mathbf{v}$ be a time-dependent vector field and

$$\varphi_{t_0}^{T}(\mathbf{x}_0) = \mathbf{x}(T) \tag{1}$$

the solution of the initial value problem

$$\dot{\mathbf{x}}(t) = \mathbf{v}(\mathbf{x}(t),t) \qquad \mathbf{x}(t_0) = \mathbf{x_0} \tag{2}$$

evaluated at $t = T$. $\varphi_{t_0}^{T}$ is called the *flow map*. Hence, the difference in position between two particles that are seeded at a small distance $\delta\mathbf{x}$ at time t_0 at time $t = T$ is given by

$$\varphi_{t_0}^{T}(\mathbf{x}_0 + \delta\mathbf{x}) - \varphi_{t_0}^{T}(\mathbf{x}_0). \tag{3}$$

Now, we apply a Taylor series expansion and get

$$\varphi_{t_0}^{T}(\mathbf{x}_0 + \delta\mathbf{x}) - \varphi_{t_0}^{T}(\mathbf{x}_0) = \varphi_{t_0}^{T}(\mathbf{x}_0) + \nabla\varphi_{t_0}^{T}(\mathbf{x}_0)\delta\mathbf{x} + R_1 - \varphi_{t_0}^{T}(\mathbf{x}_0) \tag{4}$$

with R_1 being an error term with $||R_1|| \in \mathcal{O}(||\delta\mathbf{x}||^2)$. Hence, in a small sphere around $\mathbf{x}_0$ we have the following approximation

$$\varphi_{t_0}^{T}(\mathbf{x}_0 + \delta\mathbf{x}) - \varphi_{t_0}^{T}(\mathbf{x}_0) \approx \nabla\varphi_{t_0}^{T}(\mathbf{x}_0)\delta\mathbf{x}. \tag{5}$$

The gradient of the flow map $\nabla\varphi_{t_0}^{T}(\mathbf{x}_0)$ is a linear operator. The maximal stretching of a δ-sphere around $\mathbf{x}_0$ is therefore

$$\max_{||\delta\mathbf{x}|| \leq \delta} \left(\frac{||\nabla\varphi_{t_0}^{T}(\mathbf{x}_0)\delta\mathbf{x}||}{||\delta\mathbf{x}||} \right) = \max_{||\delta\mathbf{x}||=1} \left(||\nabla\varphi_{t_0}^{T}(\mathbf{x}_0)\delta\mathbf{x}|| \right) = ||\nabla\varphi_{t_0}^{T}(\mathbf{x}_0)||_{op} \tag{6}$$

$||\cdot||_{op}$ being the operator norm with respect to the usual Euclidian norm [11]. Assuming exponential growth and scaling by the integration length we get

$$\mathrm{FTLE}(\mathbf{x}_0) = \frac{1}{|T-t_0|} \ln\left(||\nabla \varphi_{t_0}^T(\mathbf{x}_0)||_{op}\right) \tag{7}$$

The equivalence of this formulation to the standard formula found in most papers is easy to check using basic properties of the operator norm [11, 13].

We see that the impact of the gradient of the flow map tensor on the unit sphere is the crucial aspect in the analysis of local separation using FTLE. The *singular value decomposition* (SVD) is a useful tool to examine this action on the unit sphere. It is well known that a linear mapping transforms the unit sphere into an ellipsoid. The SVD gives us the opportunity to compute the main axes of this ellipsoid explicitly. More generally, the SVD of any linear mapping A is its unique representation as

$$A = U \cdot diag_0(\sigma_1, \ldots, \sigma_r, 0, \ldots, 0) \cdot V^* \tag{8}$$

where U and V are orthogonal matrices, r the rank of the matrix A, and $diag_0$ a block-diagonal matrix [11]. $(\cdot)^*$ denotes the transposition operator. In addition, the relation $\sigma_1 \geq \sigma_2 \geq \ldots \geq \sigma_r > 0$ holds. The columns of the matrix U are in the direction of the axes of the ellipsoid which the unit sphere is mapped to. The values σ_i are the lengths of its main axes and $\sigma_1 = ||A||_{op}$. Fig. 2(a) illustrates this for the linear map given by $\frac{1}{4}\left(\begin{smallmatrix}1 & 3\\ 4 & 2\end{smallmatrix}\right)$. We see that using the SVD to gain directional information about the local separation is a straight-forward extension of the original considerations of Haller.

It is worthwhile noticing that an eigenvalue decomposition of the Cauchy-Green tensor used in the standard presentation of FTLE will yield the columns of V, and not U. Unless the deformation is rotation free, these vectors will not coincide. However, the columns in V are mapped onto the columns of U. These two different sets of axes are known as the *principal spatial* and *principal material strains*, respectively. The principal material strains provide the information on the shape of the ellipse resulting from the advection of the unit sphere $\mathscr{S}^2$ by the flow. Therefore, the use of the principal material strains to gain the directional information on the FTLE field is a straight-forward extension of the geometric approach to FTLE provided by Haller in its original paper [13]. For a thorough discussion of straining we refer to Mase [22] and Hayes [16]. Given the path line γ started in $\mathbf{x}_0$ at t_0 and integrated to $t = T$, the direction of the path line at any instant t is given by $\dot{\gamma}(t) = \mathbf{v}(\gamma(t),t)$ and the corresponding separation direction $U_{-1}(t)$ (i.e, the first column of U) is computed from $\nabla \varphi_{t_0}^t(\mathbf{x}_0)$. Hence, we can use

$$\frac{1}{T-t_0} \int_{t_0}^{T} \left| \left\langle U_{-1}(t), \frac{\mathbf{v}(\gamma(t),t)}{||\mathbf{v}(\gamma(t),t)||} \right\rangle \right| \mathrm{d}t \tag{9}$$

as a measure for the directional difference between separation and path line starting in $(\mathbf{x}_0, t_0)$. Notice that perfect alignment of the separation direction and the flow direction, i.e., the situation we want to filter out, will cause the integrand to be 1. The absolute value has to be used since SVD may invert the orientation.

It is important to point out that this separation measure is not Galilean invariant, since it depends on properties such as velocity that are themselves not Galilean

invariant. The separation measure will therefore detect path lines, that are locally parallel in the chosen frame of reference. Although Galilean invariance is an important property in general flow analysis, many interesting situations with fixed frame of reference exist, e.g., fluid flow in a tube or air flow inside of a room. Besides this, we also give an example of a separation situation below, where a Galilean invariant separation measure would fail to detect a separation that can easily be deduced from the visual inspection of the path lines in the flow (see Sec. 4.1).

In practical computations, eq. (9) needs to be discretized. We now assume to have N samples of the path line $(\gamma(t_n))_{n=1}^{N}$. Since the velocities could change rapidly in direction, without actually affecting the perceived overall direction of the path line much, $\gamma(t_{i+1}) - \gamma(t_i)$ can be used instead of $\mathbf{v}(\gamma(t_{i+1}), t_{i+1})$ to robustify the measure. But even with this robustification, the local position differences can deviate substantially from the perceived overall direction, as we can see from Fig. 2(b). We therefore choose $\gamma(t_N) - \gamma(t_i)$ instead. As the approximation to the velocities, this expression is less sensitive to fluctuation in the velocity along the path line. In addition, it uses our knowledge of where the particle will end up. In this way we estimate the overall direction of the remaining trajectory. As a convenient side effect, this estimation is also less sensitive with respect to the chosen sampling of the path line (see Sec. 5). With this considerations in mind, the discrete version of our measure for spatial separation is:

$$1 - \frac{1}{N-1} \sum_{i=1}^{N-1} \left| \left\langle U_{-1}(t_i), \frac{\gamma(t_N) - \gamma(t_i)}{||\gamma(t_N) - \gamma(t_i)||} \right\rangle \right| \tag{10}$$

The main separation direction is the left-singular vector associated with the maximum singular value. The maximum singular value of the deformation gradient tensor (or, equivalently, the maximum eigenvalue of the Cauchy-Green tensor) is, however, not unique by definition. In fact, all singular values σ_i might be the same, or almost the same. In addition, numerical errors may cause the two largest singular values to be of the same order. In the original definition of FTLE this does not create any problems since we are interested in the maximum only. In contrast, when looking at the angle between the associated left-singular vector and the flow vector, this situation needs special consideration. From the SVD we know that those vectors are orthogonal to each other. Hence, even if one of the vectors is almost parallel to the flow, there is a direction of comparable distortion that is nearly orthogonal to the flow. Therefore, we shal consider these points as if the main separation occurs at a large angle to the flow direction. The consideration of the third singular value is not necessary since its left-singular vector lies in the same plane orthogonal to the first left-singular vector as the left-singular vector associated with the second singular value. To account for this, we introduce a scaling factor $1 - \frac{\sigma_2(t_i)}{\sigma_1(t_i)}$ for the single summands in eq. (10), and our final definition of the separation measure sep becomes

$$sep(\mathbf{x}_0) := 1 - \frac{1}{N-1} \sum_{i=1}^{N-1} \left(1 - \frac{\sigma_2(t_i)}{\sigma_1(t_i)}\right) \left| \left\langle U_{-1}(t_i), \frac{\gamma(t_N) - \gamma(t_i)}{||\gamma(t_N) - \gamma(t_i)||} \right\rangle \right| \tag{11}$$

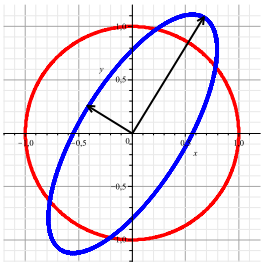

(a) Illustration of the SVD

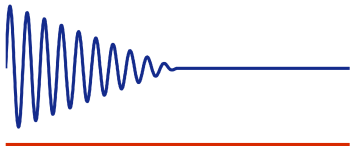

(b) two path lines with the same percieved "overall" direction (viewed from left to right)

Fig. 2 (a) Illustration of the geometric interpretation of singular values and left-singular vectors of a linear map: The unit circle (red) and its image (blue) under a linear map. The black arrow correspond to the left-singular vectors of the map, scaled by the respective singular values. (b) The figure shows the trajectories of two particles moving from left two right. Although local velocities are very different we perceive them as having the same overall direction.

Obermaier et al. [23] use the quotient of the smallest and the largest singular value to measure the overall deformation of an advection. In two dimensions, this measure coincides with the quotient in our scaling factor, the interpretation is however slightly different, as the afore reasoning shows.

The basic concept of the filtering: Bringing all this together, the proposed filter scheme can be set up by four computational steps:

1. Computation of the deformation gradient tensor: This step is generally necessary in all FTLE-related algorithms and involves the integration of path lines. We save the particle positions at some intermediate time instances as well in order to compute the spatial separation. Further details are discussed in section 5.
2. Computation of the SVD of the deformation gradient tensor: This step leads both to the FTLE field and the main separation directions.
3. Computation of the spatial separation of the flow using eq. (11).
4. Focusing on regions of large angles: This focusing can be achieved by thresholding or by smooth brushing [5].

In a final step the filter is applied to the regions with high FTLE values. The above described four steps comprise the main idea for our filtering approach.

The filter: The actual filter is then constructed by applying (smooth) brushing to the field sep. This brush maps values of the separation measure sep to the interval $[0,1]$ and describes the degree of being *in focus*. This then corresponds to accordingly modulated opacity values in the 3D view (cf. Doleisch and Hauser [5] for further details). Hence, we can formulate our filter as $filter = brush(sep)$ Eventually, this filter is then applied to the FLTE values. This focusing is done by smooth brushing as well. The overall feature characterization function f_{sep} with range $[0,1]$ (1 or near 1 for all locations in the flow which are considered to be part of the searched separation structure), is therefore described by

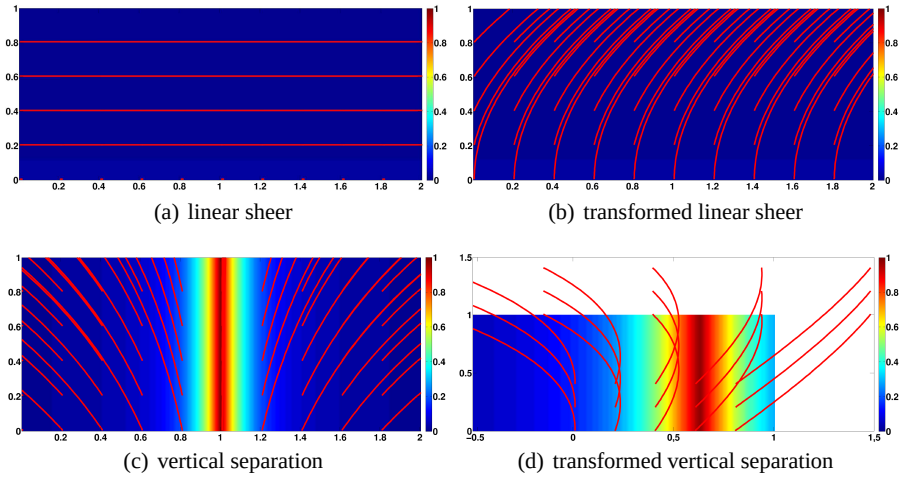

(a) linear sheer (b) transformed linear sheer

(c) vertical separation (d) transformed vertical separation

Fig. 3 Stream, resp. path, lines with the separation value as color field in the background. The left column shows the original fields, the right a Galilean transformed field. For the equations we refer to Sec. 4.1. The FTLE field is constant for all four cases. In (a) and (b) we infer from the stream lines that no spatial separation is present and the separation values are as expected close to zero (range $[0, 0.02]$). In (c) and (d) the trajectories show clear spatial separation and again the separation values coincide with the visually detected separation lines.

$$f_{sep} = brush(\mathrm{FTLE}) \cdot filter = brush(\mathrm{FTLE}) \cdot brush(sep) \tag{12}$$

The function sep can also be thought of as a degree of "featureness" for the feature "spatial separation", or, as *degree of interest* (DOI), using another terminology [5].

4 Case studies

In the following we present results from the extraction of separation structures from different data sets. We demonstrate how our filtering scheme helps to focus on regions which actually separate flow compartments that move into different regions of the flow.

4.1 Synthetic test data

First we investigate four small analytic examples where the separation behavior can be deduced directly from the equations

$$\mathbf{v}_1(x,y) = (y,0)^T, \qquad \mathbf{v}_2(x,y) = (y,1)^T \tag{13}$$

$$\mathbf{v}_3(x,y) = (x-1,1)^T, \qquad \mathbf{v}_4(x,y,t) = (x-t,1)^T \tag{14}$$

Notice that the field $\mathbf{v}_2$ arises from field $\mathbf{v}_1$ under the Galilean transformation $(x,y,t) \mapsto (x,y+t,t)$. The field $\mathbf{v}_4$, in turn, arises from $\mathbf{v}_3$ using the Galilean transformation $(x,y,t) \mapsto (x+t,y,t)$. Hence, it is easy to deduce from the fields $\mathbf{v}_1$ and $\mathbf{v}_3$ that the FTLE field is constant for all four fields. We investigate all four fields on the upper half plane (i.e., $y \geq 0$) and choose $t_0 = 0$ and $T = 1$. All computations for this example have been carried out using the MAPLE software package. The flow map was computed using MAPLEs seventh-eighth order continuous Runge-Kutta method `dverk78`. For estimation of the deformation gradient tensor we used central finite differences in the coordinate directions with spacing $h = 0.01$. For the first two fields, our separation measure *sep* is in the range $[0, 0.02]$. Hence, we expect no spatial separation. Plotting the respective stream lines of the fields shows that our filter handles both straight parallel lines (as described in the thought experiment in the introduction) as well as "locally parallel" trajectories. In contrast to the first two fields, we expect to see a clear spatial separation in the remaining two. In the first field this separation line is clearly $x = 1$, in the second field the separation line will be located right of the y-axis. Its location depends on the integration time and the speed of the observer, since this determines if particles starting on the right side of the y-axis have "enough time to turn". Our separation measure shows the expected behavior and stream, respectively path, lines plotted as a verification show the expected behavior at the separation line (see Fig. 3). The field $\mathbf{v}_4$ is an example where a Galilean invariant measure for separation would not give a response: fixing the integration time the observer speed determines where the separation line is located, and it is easy to see that any parallel to the y-axis can be achieved. Since the response would have to be the same for all observer speeds, the field would have to be constant.

4.2 Double gyre

We demonstrate our approach in context of a well-known analytic two-dimensional example, known as the "double gyre". This has been used by Shadden et al. to demonstrate the non-usability of vector field topology for time-dependent flow [29], amongst others. For the analytic definition of the field, we refer to the original paper by Shadden et al. [29]. Using the same notation as in their paper, our parameter set is $A = 1/10$, $\omega = \pi/5$ and $\varepsilon = 1/4$. The field is defined on $[0,2] \times [0,1] \times \mathbb{R}$. All computations for this example have been carried out using the MAPLE software package. The flow map was computed using MAPLEs seventh-eighth order continuous Runge-Kutta method `dverk78`, for estimation of the deformation gradient tensor we used central finite differences in the coordinate directions with spacing $h = 0.01$. Fig. 4(a) shows the FTLE field with parameters $t_0 = 0$ and $T = 15$, i.e., 1.5 periods. The filtering is emulated by setting the FTLE value of points with $sep(\mathbf{x}) \leq 0.5$ to

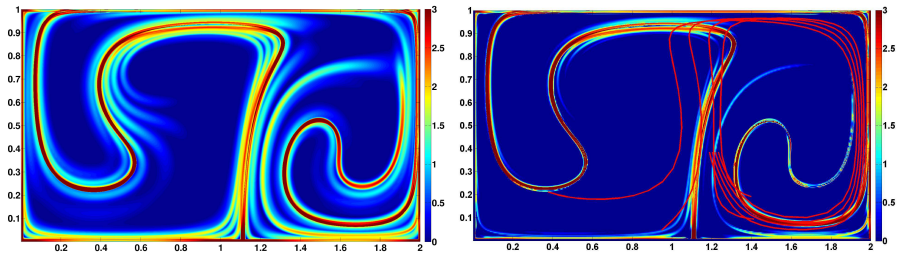

(a) FTLE field (b) filtered FTLE field

Fig. 4 The FTLE field of the double gyre with parameters $t_0 = 0$ and $T = 15$ (i.e., 1.5 periods). (a) The unfiltered field. (b) The filtered by setting FTLE values to 0 for $sep(\mathbf{x}) \leq 0.5$. Path lines confirm that the persistent ridge is indeed due to spatial separation.

0. We see that the filtering produces sharper ridges as the original FTLE field, highlighting in particular one ridge associated with rather low FTLE values. Seeding path lines at both sides of the ridge shows that the highlighted ridge is due to the desired type of separation, indeed.

4.3 A bursting dam

We apply our approach to the simulation of a bursting dam with a box-shaped obstacle. The data set consists of 48 time steps, covering the time span $[2, 120]$ (seconds) non-uniformly. The burst occurs in the first time step. We expect a recirculation zone in front (upstream) of the obstacle due to particles hitting the wall and recirculating and others getting deviated to the left and right of the obstacle. Furthermore we expect reflux on the backside of the obstacle due to pressure differences, causing particles from the end of the box to be sucked towards the obstacle, some of them ending up in front, some getting incorporated by the main flow. Right behind the obstacle we expect to see recirculation. A schematic overview of the flow can be found in Fig. 5(a). The SimVis framework [4] was used for this example. We calculated the FTLE field for $t_0 = 62$ and $T = 68$, using the optimal 4^{th} order Runge-Kutta method (sometimes referred to as the "3/8-rule"). For details we refer to Hairer et al. [12]. The usage of a even higher order integration method (which is not standard) was purely due to the fact the MAPLE software package readily provides this method. The integration time was found empirically with the aim that not more that 15 percent of the particles seeded leave the flow domain before the end of the integration time. Fig. 5(b) shows an overview over the FTLE field. We filter the field brushing all points with a *sep*-value greater or equal 0.45 (smooth lower bound 0.4). We will now investigate two regions in the flow domain more closely: The region stream-wise in front of the obstacle and the upper rear region.

(a) Schematic overview (b) FTLE field

Fig. 5 (a) Schematic overview over the flow domain, z being the streamwise direction. (b) The FTLE field of a simulation of a bursting dam with parameters $t_0 = 62$ and $T = 68$. The FTLE values greater than 0.25 are brushed (smooth lower bound 0.2) . We see that we can identify expected structures around the obstacle. The upper rear part of the flow domain shows large regions with high FTLE values, presumably induced by shearing.

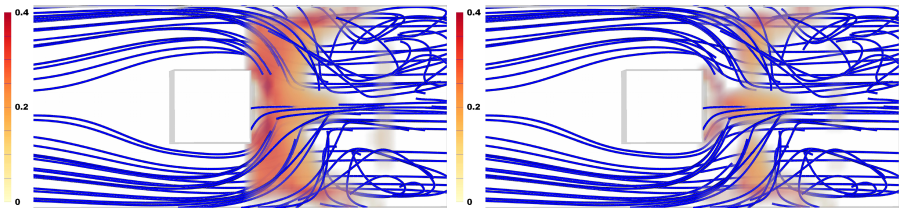

(a) FTLE field (b) filtered FTLE field

Fig. 6 The (a) FTLE and (b) filtered FTLE field upstream (right in the figures) of the obstacle in top view. The FTLE values greater than 0.25 are brushed (smooth lower bound 0.2), $sep(\mathbf{x}) < 0.45$ (smooth lower bound 0.4) is used for the filtering in (b). We see that the spatial separation structure stemming from particles passing on different sides of the obstacle is not clearly discernible in the unfiltered field. While adjusting the brush would not give the desired structure either, our filtering does.

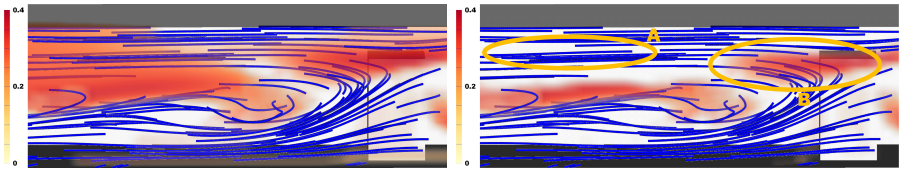

(a) FTLE field (b) filtered FTLE field

Fig. 7 A cross section of the (a) FTLE and (b) filtered FTLE field. The filtering used is the same as in fig. 6. The ellipse (A) shows a region where the filter has a strong impact. We see that the path lines are locally parallel and show little to no spatial separation. In contrast, we see that the structure below the ellipse separates path lines moving from the left to the right (above) from those moving in the opposite direction (below). In the same fashion, the ellipse (B) indicates a structure that separates particles coming from the left and passing over the obstacle, from those moving back to the left end of the flow domain. This structure is persistent under our proposed filter.

In front of the obstacle: In front of the obstacle, we expect to detect a separation structure upstream, due to particles passing on different sides of it. We see that (Fig. 6(a)) this expected separation structure is not detectable from the original field. Applying our separation filter allows us to focus on this spatial separation,

	$N=$	2	4	6	8	10
$\mathbf{v}_4$	mean	$1.2\cdot10^{-3}$	$6.13\cdot10^{-4}$	$3.23\cdot10^{-6}$	$1.64\cdot10^{-5}$	$3.5\cdot10^{-5}$
	variance	$1.27\cdot10^{-6}$	$3.04\cdot10^{-7}$	$8.42\cdot10^{-7}$	$2.17\cdot10^{-8}$	$3.5\cdot10^{-9}$
double gyre	mean	0.2	0.1	0.07	0.04	0.01
	variance	0.03	0.01	0.03	$9.4\cdot10^{-4}$	$1.4\cdot10^{-4}$
breaking dam	mean	$1.27\cdot10^{-2}$	$5.47\cdot10^{-3}$	$2.57\cdot10^{-3}$	$9.82\cdot10^{-4}$	$6.6\cdot10^{-5}$
	variance	$1.13\cdot10^{-5}$	$2.4\cdot10^{-7}$	$5.36\cdot10^{-8}$	$7.7\cdot10^{-9}$	$2.97\cdot10^{-9}$

Table 1 Error Analysis of Sampling Density

even though the corresponding FTLE values do not show up prominently in the original field. We added path lines to both figures to confirm that the intuitively expected separation structure indeed exists and coincides with the structure found by the filtering with our separation measure.

The upper rear region: In the overview in fig. 5(b) we see a large region with high FTLE in the upper rear part of the flow domain. Applying our filtering reduces the region to a surface separating particles moving from the back to the front (upper part) from those leaving the flow domain (lower part). We seeded particles in a cross-section in order to validate the result from the filtering. We see that the particles in the region delineated by the ellipse (A) in fig. 7(b) show the expected locally parallel pattern. The structure at approximately half height of the box captures the boundary between the two essentially different particle behaviors described above. The structure in ellipse (B) in fig. 7(b) separates particles moving from the back to the front and passing over the obstacle from those inverting their motion direction again. This separation is again the type our filter aims to focus on.

5 Computational Issues

Although the steps that are needed to compute the proposed filter are in theory rather straightforward, the application to discrete data offers some challenges we want to discuss. Namely, we address (a) the influence of the used sampling of the path line, and (b) the computational cost of computing the FTLE field following our suggestions compared to the standard algorithm.

The impact of the sampling: Our sampling of the path line at $\frac{1}{2},\frac{3}{4},\frac{7}{8}$ and the full integration time puts emphasis on the end of the path lines. Visually, this is intuitive, since we perceive path lines as parallel if their ends show this behavior. We anticipate common "spatial fate". Therefore will rather small direction changes towards the end of the registered path lines intuitively be read as diverging behavior, since we anticipate that the motion will continue in the same direction.

We computed the separation measure for some of the data sets, namely the time-dependent ones, for $N=2,4,6,8,10$ and compared the results point-wise, using the N=25 as reference value. Table 1 shows the average relative error and the variance in the computed fields. We chose to investigate the time-dependent data sets since

this is most relevant in practice because FTLE computations for steady fields are usually avoided using vector field topology instead.

FTLE as eigenvalues of the Cauchy-Green tensor vs. singular values of the deformation gradient tensor: Our filtering needs, in addition to the FTLE field, the left-singular vectors of the deformation gradient tensor. This is not a part of the usual algorithm to compute FTLE. However, the computation of the deformation gradient tensor is. Therefore, we do an informal comparison of the expected computational cost. Essentially, the here used alternative FTLE computation methods differ from the standard method in one aspect only: the use of the SVD instead of the eigenvalue decomposition. Standard algorithms for both decompositions are based on the same transformation in the iteration steps and have therefore the same complexity order. The singular matrices are an by-product of the SVD computation and do not need to be computed separately. For details we refer to Gill et al. [9]. Hence, computing the FTLE plus left-singular vectors will not be substantially slower than the usual computation of FTLE from the Cauchy-Green tensor. With the Maple implementations of SVD and eigenvalue decomposition the ratio of the computation time using the SVD to the time used with the standard formula is in the range $[0.95, 1.06]$, i.e., the SVD-based method is in the worst case 6% slower than the standard method on the double gyre data set. In SimVis we used the linear algebra library *JAMA* (`http://math.nist.gov/tnt/overview.html`), which gives a ratio of 1.12 for the bursting dam data set, i.e., a 12% computational overhead. It is worthwhile noticing that our methods provides both the regular FTLE field plus the additional information needed to perform the filtering at once. Hence, ridge extraction algorithms may be applied as well, if wanted.

6 Discussion and future work

We examine the results from analyzing several different flow scenarios with the here proposed filtering scheme. We assess the filtered structures by seeding path lines in the unfiltered field and comparing the result of our filtering scheme to the result that we would expect from the path lines. In all cases the paths lines seeded in the filtered region show the expected locally parallel flow pattern (which we see as a satisfying confirmation of our more theoretical considerations with respect to the design of the proposed filter).

The computation of the flow map is, as expected, the bottle neck when applying our filtering to data sets. A speed-up of this computation could be achieved by exploiting the inherent parallel nature of path line computation and multi-core architectures. AMR and advection based methods to speed-up computations do not seem to be suitable at the first sight, since we are not extracting ridges and we do not know whether the structures that our filtering reveals have properties corresponding to material lines and surfaces. We intend to perform computational experiments to assess this question.

Finally, we intend to assess the effects of combining our filtering with other flow feature detectors. FTLE is known to miss out on some features as, for example, vortices. Hence, the combination of feature detectors is a promising approach [2, 3]. We have implemented our filtering in the SimVis framework [4], that is inherently suitable for the proposed investigation due to its combination of interactive visual analysis and 3D context visualization designed for flow data.

FTLE based methods, and consequently also our filtering of the field, are known to be heavily dependent on the choice of the integration length [8, 29]. Hence, the search for separation measures that can handle diverging and re-converging flow (as in flow around an obstacle) and similar behavior seems appealing.

7 Conclusion and Acknowlegdments

In this paper we discuss two different types of separation and showed how to distinguish them filtering *finite-time Lyaponov exponents*. Analyzing different flow scenarios, we showed that this distinction indeed yields a deeper understanding of separation structures. Separation is an important aspect in flow analysis and further classification of different types of this phenomenon seems to be a promising research direction.

The project SemSeg acknowledges the financial support of the Future and Emerging Technologies (FET) programme within the Seventh Framework Programme for Research of the European Commission, under FET-Open grant number 226042.
The CFD simulation of a bursting dam is courtesy of AVL List GmbH, Austria.

References

1. Asimov, D.: Notes on the topology of vector fields and flows. Tech. rep., NASA Ames Research Center (1993). RNR-93-003
2. Bürger, R., Muigg, P., Doleisch, H., Hauser, H.: Interactive cross-detector analysis of vortical flow data. In: Proc. of the 5th Int'l Conf. on Coordinated & Multiple Views in Exploratory Visualization (CMV 2007), pp. 98–110 (2007)
3. Bürger, R., Muigg, P., Ilčík, M., Doleisch, H., Hauser, H.: Integrating local feature detectors in the interactive visual analysis of flow simulation data. In: K. Museth, T. Möller, A. Ynnerman (eds.) Data Visualization 2007: Proc. of the 9th Joint EUROGRAPHICS – IEEE VGTC Symp. on Visualization (EuroVis 2007), pp. 171–178. A K Peters (2007)
4. Doleisch, H.: SimVis: Interactive visual analysis of large and time-dependent 3D simulation data. In: Proc. of the 2007 Winter Conf. on Simulation (WSC 2007), pp. 712–720 (2007)
5. Doleisch, H., Hauser, H.: Smooth brushing for focus+context visualization of simulation data in 3D. Journal of WSCG **11**(1-2), 147–154 (2001)
6. Fuchs, R., Kemmler, J., Schindler, B., Waser, J., Sadlo, F., Hauser, H., Peikert, R.: Toward a lagrangian vector field topology. Computer Graphics Forum **29**(3), 1163–1172 (2010)
7. Garth, C., Gerhardt, F., Tricoche, X., Hagen, H.: Efficient computation and visualization of coherent structures in fluid flow applications. IEEE Transactions on Visualization and Computer Graphics **13**(6), 1464–1471 (2007)

8. Garth, C., Li, G.S., Tricoche, X., Hansen, C.D., Hagen, H.: Visualization of coherent structures in transient 2D flows. In: H.C. Hege, K. Polthier, G. Scheuermann (eds.) Topology-Based Methods in Visualization II: Proc. of the 2nd TopoInVis Workshop (TopoInVis 2007), pp. 1–13 (2009)
9. Gill, P.E., Murray, W., Wright, M.: Numerical Linear Algebra and Optimization, 1st edn. Addison Wesley Publishing Company (1991)
10. Globus, A., Levit, C., Lasinski, T.: A tool for visualizing the topology of three-dimensional vector fields. In: Proc. of IEEE Visualization '91, pp. 33–40 (1991)
11. Golub, G.H., Van Loan, C.F.: Matrix Computations, 3rd edn. Johns Hopkins Studies in Mathematical Sciences. The Johns Hopkins University Press (1996)
12. Hairer, E., Nørsett, S.P., Wanner, G.: Solving Ordinary Differential Equations I, 2nd edn. Springer Series in Computational Mathematics. Springer (1993)
13. Haller, G.: Distinguished material surfaces and coherent structures in three-dimensional fluid flows. Physica D **149**, 248–277 (2001)
14. Haller, G.: Lagrangian coherent structures from approximate velocity data. Physics of Fluids **14**, 1851–1861 (2002)
15. Haller, G., Sapsis, T.: Lagrangian coherent structures and the smallest finite-time lyapunov exponent. Chaos (2010)
16. Hayes, M.: On strain and straining. Archive for Rational Mechanics and Analysis **100**(3), 265–273 (1988)
17. Helman, J., Hesselink, L.: Representation and display of vector field topology in fluid flow data sets. IEEE Computer **22**(8), 27–36 (1989)
18. Helman, J., Hesselink, L.: Visualizing vector field topology in fluid flows. IEEE Computer Graphics and Applications **11**, 36–46 (1991)
19. Jordan, D.W., Smith, P.: Nonlinear ordinary differential equations : an introduction for scientists and engineers, 4th ed. edn. Oxford Applied and Engineering Mathematics. Oxford University Press (2007)
20. Kasten, J., Petz, C., Hotz, I., Noack, B., Hege, H.C.: Localized finite-time Lyapunov exponent for unsteady flow analysis. In: Vision Modeling and Visualization, pp. 265–274 (2009)
21. Lipinski, D., Mohseni, K.: A ridge tracking algorithm and error estimate for efficient computation of Lagrangian coherent structures. Chaos **20**(1), 017,504 (2010)
22. Mase, G.E.: Continuum Mechanics, 1st edn. Schaum's Outline Series. McGraw-Hill (1969)
23. Obermaier, H., Hering-Bertram, M., Kuhnert, J., Hagen, H.: Volume deformations in grid-less flow simulations. Computer Graphics Forum **28**(3), 879–886 (2009)
24. Perry, A., Chong, M.: Topology of Flow Patterns in Vortex Motions and Turbulence. Applied Scientific Research **53**, 357–374 (1994)
25. Pobitzer, A., Peikert, R., Fuchs, R., Schindler, B., Kuhn, A., Theisel, H., Matković, K., Hauser, H.: On the way towards topology-based visualization of unsteady flow - the state of the art. In: Eurographics 2010 – State of the Art Reports. Eurographics Association (2010)
26. Sadlo, F., Peikert, R.: Efficient Visualization of Lagrangian Coherent Structures by Filtered AMR Ridge Extraction. IEEE Transactions on Visualization and Computer Graphics **13**(6), 1456–1463 (2007)
27. Sadlo, F., Peikert, R.: Visualizing Lagrangian coherent structures: A comparison to vector field topology. In: H.C. Hege, K. Polthier, G. Scheuermann (eds.) Topology-Based Methods in Visualization II: Proc. of the 2nd TopoInVis Workshop (TopoInVis 2007), pp. 15–29 (2009)
28. Sadlo, F., Peikert, R.: Time-dependent visualization of Lagrangian coherent structures by grid advection. In: V. Pascucci, X. Tricoche, H. Hagen, J. Tierny (eds.) Topological Methods in Data Analysis and Visualization: Theory, Algorithms and Applications. Springer (2011)
29. Shadden, S., Lekien, F., Marsden, J.: Definition and properties of Lagrangian coherent structures from finite-time Lyapunov exponents in two-dimensional aperiodic flows. Physica D Nonlinear Phenomena **212**, 271–304 (2005). DOI 10.1016/j.physd.2005.10.007
30. Shi, K., Theisel, H., Weinkauf, T., Hege, H.C., Seidel, H.P.: Visualizing Transport Structures of Time-Dependent Flow Fields. Computer Graphics and Applications **28**(5), 24–36 (2008)

31. Theisel, H., Weinkauf, T., Hege, H.C., Seidel, H.P.: Topological methods for 2D time-dependent vector fields based on stream lines and path lines. IEEE Transactions on Visualization and Computer Graphics **11**(4), 383–394 (2005)
32. Wasberg, C.E.: Post-processing of marginally resolved spectral element data. In: J.S. Hesthaven, E.M. Rønquist (eds.) Spectral and High Order Methods for Partial Differential Equations, *Lecture Notes in Computational Science and Engineering*, vol. 76, pp. 503–510. Springer Berlin Heidelberg (2011)
33. Wiebel, A., Chan, R., Wolf, C., Robitzki, A., Stevens, A., Scheuermann, G.: Topological Flow Structures in a Mathematical Model for Rotation-Mediated Cell Aggregation. In: V. Pascucci, X. Tricoche, H. Hagen, J. Tierny (eds.) Topological Methods in Data Analysis and Visualization: Theory, Algorithms and Applications. Springer (2011)